Chemical Papers (2025) 79:1087–1101
https://doi.org/10.1007/s11696-024-03842-3

ORIGINAL PAPER

Glycine-modified chitosan-embedded silver nanoparticles: a green approach to Pb^{2+} adsorption and bioactivity enhancement

Suba Kannaiyan[1] · Andal Gopal[2] · R. Lakshmipathy[3] · Daoud Ali[4] · Saud Alarifi[4] · Mithra Geetha[5] · Kishor Kumar Sadasivuni[5,6]

Received: 6 October 2024 / Accepted: 29 November 2024 / Published online: 10 December 2024
© The Author(s) 2024

Abstract

Glycine-modified chitosan anchored silver nanoparticles (SCG) were synthesized using a green method without a cross-linking agent. UV–Vis, FTIR, XRD, TEM and SEM techniques confirmed the formation of the SCG nanocomposite and silver nanoparticles. The SCG nanoparticles, estimated at 20 nm, are smaller than the chitosan stabilized Ag (SC) nanoparticles. The biological significance of the SCG nanoparticles was assessed through their anti-oxidant and antibacterial activities. SCG nanoparticles demonstrated significant anti-oxidant activity with an IC50 of 133 µg ml^{-1}, surpassing that of SC nanoparticles. The ZoI of was found to be 30 mm for the S. aureus and E. coli bacterial strains indicating excellent antimicrobial activity. The efficiency of SCG nanoparticles in removing Pb^{2+} ions was tested using a batch adsorption process. A Central Composite Design (CCD) was employed to optimize the independent variables, and ANOVA results indicated the CCD model's reliability and significance with a p-value < 0.0001. The SCG nanoparticles exhibited a high Pb^{2+} ion loading capacity of 270.2 mg g^{-1} from aqueous solution with a removal efficiency of 93%. Isotherm and kinetic investigations of the equilibrium data suggest the suitability of Langmuir and pseudo-second-order kinetic models. Thermodynamic studies revealed the process's spontaneity and exothermic nature. The mechanism of adsorption was found to be ion exchange with a mean potential energy (E_s) of 9.4 kJ/mol. These findings suggest that glycine-modified chitosan anchored silver nanoparticles have promising applications in biological and environmental domains.

Keywords Silver nanoparticles · Anti-oxidant · Antibacterial · Adsorption · RSM

Introduction

Noble metal nanoparticles have captivated researchers for over a century due to their potential applications in biomedical sciences and engineering. Silver nanoparticles, in particular, stand out for their unique surface plasmon properties and therapeutic applications. Various physicochemical techniques have been employed to synthesize silver nanoparticles. However, these methods often involve the use of toxic chemicals, as well as high energy, temperature, and pressure requirements, which can be detrimental to the environment (Hassan et al. 2024; Lena 2023; Sharma et al. 2009; Ohiduzzaman et al. 2024). The biological method of synthesizing silver nanoparticles is regarded as an economical and environmentally friendly alternative to physicochemical approaches (Azmi et al. 2021). Biopolymers, a diverse group of naturally occurring polymers, include examples such as starch and cellulose, which are commonly used in various household products. Researchers are intrigued by a

✉ R. Lakshmipathy
lakshmipathy.vit@gmail.com

✉ Kishor Kumar Sadasivuni
kishor_kumars@yahoo.com

[1] Department of Chemistry, Sri Sairam Engineering College, Chennai, India

[2] Department of Chemistry, KCG College of Technology, Chennai, India

[3] Directorate of Learning and Development, SRM Institute of Science and Technology, Kattankulathur, Tamil Nadu, India

[4] Department of Zoology, College of Science, King Saud University, Riyadh, Saudi Arabia

[5] Center for Advanced Materials, Qatar University, Doha, Qatar

[6] Department of Mechanical and Industrial Engineering, Qatar University, Doha, Qatar

recent discovery in polymer solutions where tiny pockets, smaller than a billionth of a meter, naturally form within the material. These pockets result from the intramolecular and intermolecular interactions of the polymer molecules. This discovery could prove valuable for the creation and stabilization of nanoparticles (Mrinalini and Mallika 2024; Mengistu et al. 2024).

The chemistry of the surface, particle size, choice of reducing and capping agents, and other factors involved in the production of silver nanoparticles all influence their biological activity. Nanoparticles based on biopolymers are anticipated to exhibit novel antimicrobial properties that could be leveraged for various therapeutic applications (Seid et al. 2023). Silver nanoparticles have been successfully reduced and stabilized using a range of natural biopolymers.

Chitosan (CS), a natural and renewable polymer obtained by the deacetylation of chitin, which is found in shellfish, fungi, and plant cell walls (Pradip et al. 2004; Prasitsilp et al. 2000), has garnered considerable attention. Due to its polymeric structure, chitosan interacts effectively with negatively charged molecules and other polymers. This property makes it an excellent agent for synthesizing metal nanoparticles, as its amino groups interact with nanoparticles to enhance control over synthesis (Wen et al. 2015). Additionally, chitosan's notable biological properties make it a promising candidate for use in drug delivery systems in the pharmaceutical and biomedical sectors (Illum 1998; Kumar and Muzzarelli 2004; Azza xxxx; Panos and Acosta 2008).

Numerous studies have been conducted on the use of chitosan as a drug delivery carrier (Nafisur and Nabila 2023). The bioactivity of chitosan can be enhanced through functionalization with bioactive molecules, such as amino acids. Amino acids are fundamental building blocks of life, composed of three essential parts: a basic amine group, an acidic carboxylic acid group, and a unique side chain that varies between amino acids. The general chemical structure of an amino acid is represented as $H_2NCHRCOOH$, where "R" denotes the variable side chain (Varshosaz 2007). The literature has reported on the chemical modification of chitosan with glycine using cross-linking agents such as thionyl chloride, phosphoryl chloride, glutaraldehyde, or epichlorohydrin (Madihally and Matthew 1999).

The presence of heavy metal ions in aqueous ecosystems is carcinogenic and poses significant risks to aquatic species. Lead (Pb) is recognized as one of the most harmful heavy metal ions, seriously contaminating and degrading aquatic environments (Mahdi et al. 2020). Various industrial processes contribute to the release of Pb^{2+} ions through effluents, which must be properly treated before being discharged into water bodies. Adsorption is considered a promising technique for the removal of Pb^{2+} ions from aqueous solutions, and the use of Response Surface Methodology (RSM) to optimize the conditions enhances the reliability and efficiency of the process (Nafisur et al. 2021, 2024). Chitosan and silver nanoparticles have been reported as effective agents for wastewater remediation, particularly in the removal of heavy metal ions from water (Huacai et al. 2016; Hosseini et al. 2016). The combination of chitosan and silver nanoparticles with surface functionalization presents an intriguing nanocomposite solution for addressing Pb^{2+} ion contamination in water bodies.

To enhance the bioactivity of nanomaterials and improve the efficiency of heavy metal ion adsorption, chitosan was modified in situ with glycine and embedded with silver nanoparticles. The nanoparticles were tested for their antibacterial effects against gram-positive and gram-negative bacteria. Further, anti-oxidant and anti-fungal activities were tested. To diversify the applications, the nanocomposite was evaluated for its ability to adsorb Pb^{2+} ions from aqueous solution. The independent variables will be optimized with RSM technique and verified statistically for its significance.

Materials and methods

Chemicals

Sodium hydroxide, glycine, $AgNO_3$, chitosan (molecular weight: 150,000, 1.5%w/v) and starch were procured from SD Fine Ltd and used as received, requiring no additional purification.

Synthesis of starch-capped silver nanoparticle

A solution of alkali-dissolved starch was prepared by dissolving 2.5 g of starch in 40 ml of water containing 0.018 g of sodium hydroxide. After the complete dissolution of starch, the solution was heated at 70 °C, and the pH observed was 12. Then 0.0175 g of $AgNO_3$ dissolved in 20 ml was added dropwise to the starch solution. The formation of a dark brown color solution with the addition of silver nitrate solution indicates that starch-capped nanoparticles were formed.

Synthesis of chitosan–glycine framework anchored silver nanoparticle

First, 5 ml of chitosan (1w/v%) solution was added to the step 1 product, and it was agitated for 15 min. After that, the mixture was agitated for 30 min; while, 5 ml of glycine (1 g) solution was added. The mixture was filtered and cleaned with distilled water following the reaction. The reaction route is displayed in the scheme formation of SC and SCG in Figs. 1 and 2.

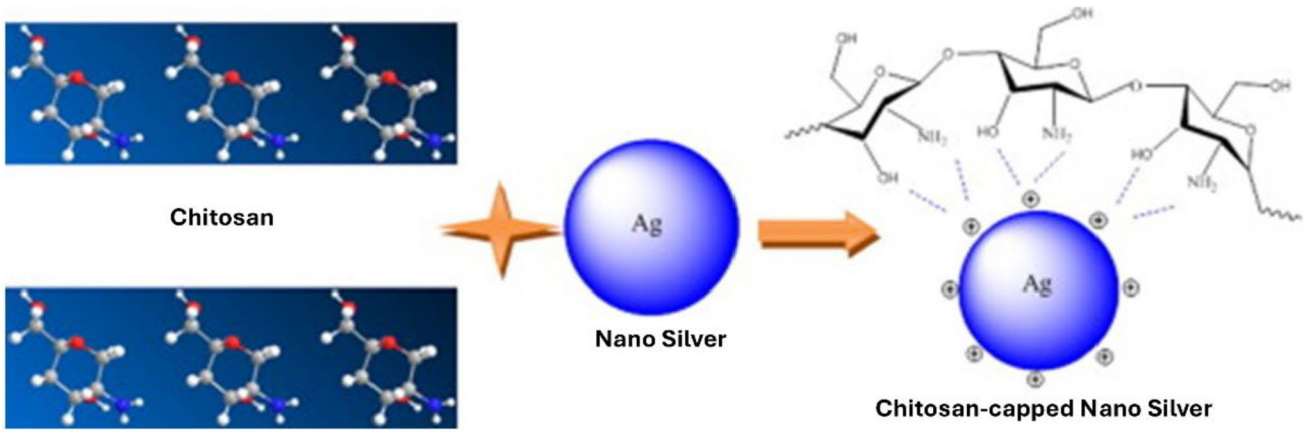


Fig. 1 Scheme of formation of Chitosan Capped Silver nanoparticle (SC)

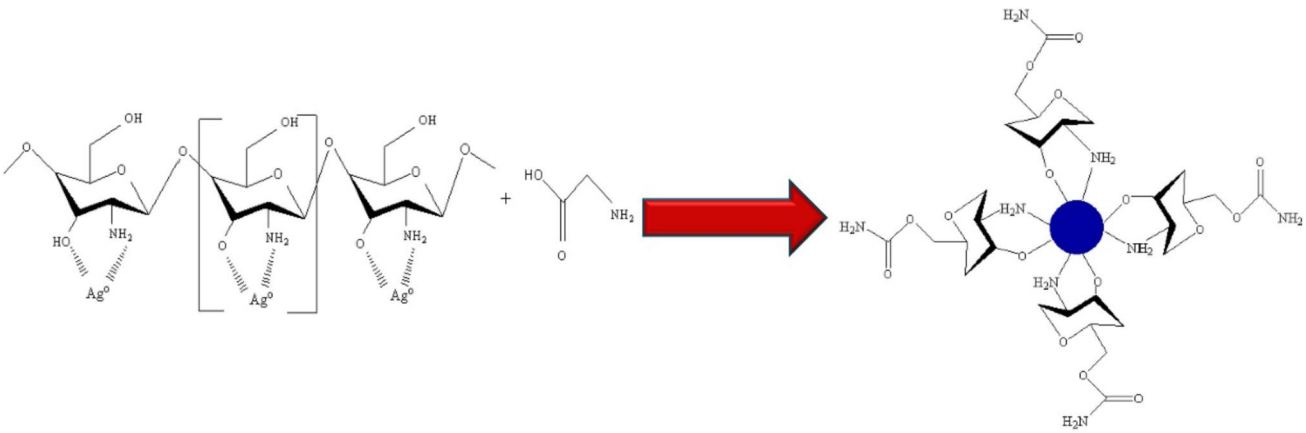


Fig. 2 In situ modification of chitosan with glycine over silver nanoparticle without any cross-linking agents (SCG)

Antimicrobial activity

The antimicrobial activity of SC, SCG was tested using the agar well diffusion method. The SC and SCG were tested in vitro for their antibacterial activity using the nutrient agar method against *Staphylococcus aureus* (MTCC430) and *Escherichia coli* (MTCC739). The anti-fungal activity was carried out against *Aspergillus fumigates* MTCC 343 and *Candida albicans* MTCC227 using Sabouraud dextrose agar medium. Gentamycin and Ketoconazole were used as conventional medications with anti-fungal and antibacterial properties. Investigations were performed in a petri dish, and used a sterile cork borer to punch out tiny wells in the agar medium, creating individual testing zones. Precise amounts (10, 20, 30, and 40 µl) of the test compounds were then carefully added into these wells using sterilized droppers. To allow the compounds to disperse evenly throughout the agar and interact with any present bacteria or fungus, the plates were left undisturbed at room temperature for two hours. The plates were allowed to incubate for 18–24 h at 37 °C. in case of antibacterial activity and 48 h at 27 °C for anti-fungal activity.

Anti-oxidant activity

The SC and SCG anti-oxidant capacity were evaluated by measuring its ability to donate hydrogen atoms or scavenge free radicals. Methanol was used to dilute the sample extracts at different concentrations (50–250 µl) until a consistent volume of 100 µl was achieved. The mixture was then mixed with 5 ml of a 0.1 mM methanolic solution of DPPH. The combination was allowed to stand at 27 °C for 20 min, and then the absorbance at a wavelength of 517 nm was measured. Based on this absorbance reading, the percentage of free radicals scavenged by the sample was calculated by below equation:

$$\%\text{DPPH radical scavenging activity} = \left(\frac{\text{Control OD} - \text{Sample OD}}{\text{Control OD}}\right) \times 100 \quad (1)$$

Each experiment was repeated three times (in triplicate) to ensure accuracy. A graph was plotted showing the percentage of inhibition versus the sample concentration. This graph calculated the specific concentration of the sample required to inhibit free radicals by 50%. This concentration is referred to as the IC50 value.

Characterization

A Hitachi U-2800 UV–Vis spectrophotometer was used to analyze the formation of Glycine-modified Chitosan anchored Silver nanoparticles. The obtained colloids were centrifuged, dried and analyzed by FTIR (FTIR spectrometer-Thermo Nicolate Company Avatar 330), SEM (PhilipsCM200 at 200 kV), TEM (JEOL Japan, JEM-2100 Plus) and Powder X-ray diffraction (Cu Ka, P Analytical).

Lead adsorption studies

The Pb^{2+} ions removal by SCG was performed in batch process by varying the independent variables such as pH, contact, time, initial concentration and temperature. All the experiments were performed in 50 ml test solutions in 100 ml conical flask and agitated at 100 rpm. The test mixtures were separated by centrifugation at 10,000 rpm and the supernatant solutions were subjected to Atomic absorption spectrometer to estimate the residual concentration of Pb^{2+} ions. The percentage removal and adsorption capacity was estimated with the following equations (Huacai et al. 2016):

$$\%Pb^{2+}\text{ion removal} = \frac{C_0 - C_1}{C_0} \times 100 \tag{2}$$

$$\text{Adsorption capacity} = \frac{C_0 - C_1}{m} \times V \tag{3}$$

Response surface methodology

A statistical technique called Response Surface Methodology (RSM) is used to create and optimize variables that affect how well adsorbents remove adsorbate ions. In view of optimizing the independent variables, a Central Composite Design (CCD) of RSM was developed considering three independent variables such as pH, contact time and initial concentration of Pb^{2+} ions using Design Expert 12.0 software. The design matrix and levels of independent variables A-pH, B-contact time and C-initial concentration are summarized in Table 1. The CCD has a total of 20 runs comprising 6 axials, 6 center and 8 factorial points executed by varying the independent variables. A quadratic polynomial coded equation representing the interaction of independent variables for the optimal removal of Pb^{2+} ions by SCG is given below

Table 1 Independent variable levels and design matrix

Variables	Symbol	Levels		
		−1	0	+1
pH	*A*	4	6	8
Contact time	*B*	30	60	90
Initial concentration	*C*	50	100	150

$$\%\ \text{Removal} = 82.58 + 6.76A + 4.32B - 9.38C + 0.33AB - 4.66AC - 0.93BC - 28.07A^2 - 2.15B^2 - 4.66C^2 \tag{4}$$

Results and discussion

The objective is to develop silver nanoparticles modified with chitosan stabilized Glycine that have enhanced antibacterial activity without using any cross-linking agents. Figures 1 and 2 depict the synthesis of the derived nanomaterial.

Characterization of chitosan-stabilized silver (SC) and glycine-modified chitosan-stabilized silver (SCG)nanoparticles

UV–Vis Spectroscopy was utilized to characterize the production of silver nanoparticles. Visual observation revealed that the solution had turned from colorless ($AgNO_3$) to brown, confirming the synthesis of starch-modified Ag NPs. After the chitosan solution was added, the brown hue persisted. The silver nanoparticles grafted with chitosan exhibited an absorbance of approximately 427 nm. After the addition of glycine to the chitosan-stabilized silver Nano colloid, the increase in intensity of the SPR Peak is observed, as shown in Fig. S1 . This may be due to the change in the silver's dielectric constant because of glycine's adsorption on the chitosan (Mohammed et al. 2017a ; Suba et al. 2022). Similar outcomes in the fabrication of chitosan-capped silver nanoparticles were reported by Praveenkumar et al. (2014). The quantum confinement effect is thought to cause the absorption peak's blue shift. Glycine can provide steric stabilization in the nanocomposite preventing agglomeration. The presence of glycine reduces inter-particle interactions, which is essential for achieving smaller and more uniform particle size of the nanocomposite (Balalakshmi et al. 2020 ; Constantin et al. 2023).

The molecular interaction of chitosan and glycine with silver nanoparticles can be ascertained from the FTIR data. The peaks at 3437 corresponds to the –OH stretching

Table 2 Vibrational frequencies of SC, SCG and unmodified nanoparticles

Vibrations	Unmodified nanoparticle	Chitosan stabilized silver nanoparticle	Glycine-modified chitosan
Overlapping of stretching of O–H and N–H bonds	3437	3437	3423
CH stretching	2922	2912	2918
Stretching of C=O secondary amide bonds	1631	1710	1562

vibrations and 2922 corresponds to the –C–H stretching vibrations of the R group. When comparing silver nanoparticles with and without chitosan modification, a minor change in the typical absorption peaks was observed (Fig. S2) (Table 2). The shift is brought on by the contact of the chitosan's hydroxylic group with the silver nanoparticles, which supports that interaction. Each chitosan monomer is joined to a silver atom via a hydroxylic group. Because chitosan's hydroxylic groups function as coordination sites, they initiate the nucleation process that results in chitosan-capped silver nanoparticles. The few literatures show similar outcomes (El-Naggar et al. 2018; Kamlesh and Usha 2011; Shahid et al. 2024).

Similar shifts are observed when glycine is modified to chitosan, and they are at wavenumbers 3423, 2918, and 1562 cm^{-1}, respectively. These shifts show that chitosan and glycine are cross-linked. The shift is noticed due to an interaction between the free end of the amine group in chitosan and the carboxylic group in glycine (Gupta et al. 2015; Mohammed et al. 2017b). The crystal size and structure of the unmodified Ag Nps, SCAg NPs, and SCG Ag NPs were examined using XRD.

The peaks for chitosan have submerged, and crystallinity has improved due to the modification of glycine moiety over chitosan. Due to polymers (starch and chitosan), the broad peak was observed at $2\Theta = 20–28$ due to the cellulose structure. The distinctive polymer peak further indicates that the surface of the synthesized particles is coated with an organic layer. The XRD pattern showed a significant peak at positions 38, 44, 64, and 74, which can be attributed to the silver face-centered cubic planes (JCPDS file No 01–071-4613). These peaks' clarity suggests that the produced particles are extremely crystalline. Smaller sizes are indicated by the broadness of the peaks (Fig. S3).

Microstructure of the nanoparticles was revealed by SEM. The initial appearance seems to be flakes like structure and in the solid phase the materials seems to be agglomerated. Similar to the pure chitosan, the silver-capped chitosan nanoparticles exhibited rough membrane-like morphology with more accumulation as seen in Fig. 3. To determine the exact size and shape of the SCG other microscopy techniques will be helpful.

Upon addition of glycine to the silver-capped chitosan nanoparticles, more uniform spherical-shaped particles are observed, confirming that chitosan is chemically cross-linked to glycine successfully. Utilizing a transmission electron microscope (TEM), the dimensional study of the synthesized SC and SCG NPs was done. Figure 4 of the TEM images showed that spherically shaped nanoparticles formed in both samples. The dispersion of Silver nanoparticles in chitosan was little agglomerated compared to glycine-modified chitosan. As the derivatives of chitosan always show unique properties, the SCG nanoparticle also have reduced size and enhanced efficacy.

Antimicrobial activity of chitosan capped silver (SC) and glycine-modified chitosan-stabilized silver (SCG)Nanoparticles

The results of the investigation into the antibacterial activity of SC and SCG against gram-positive *Escherichia coli*

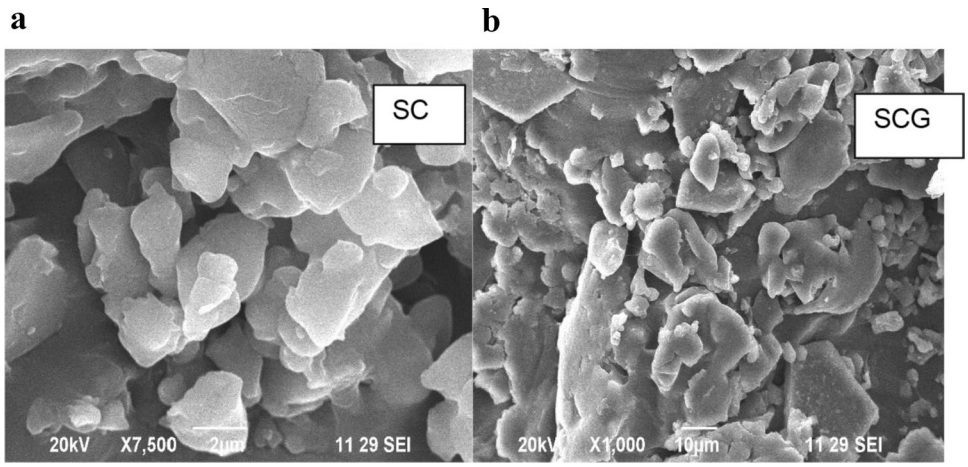


Fig. 3 SEM image of **a** SC **b** SCG

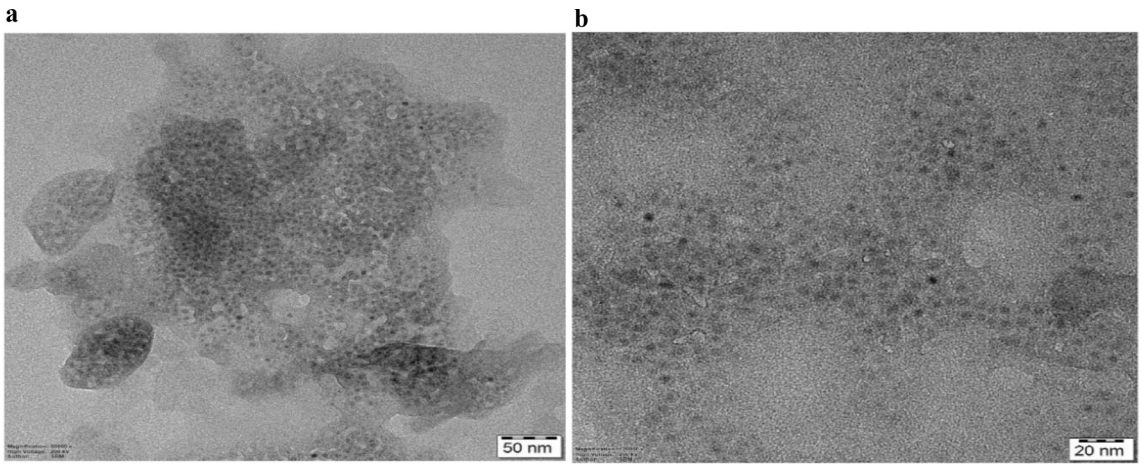


Fig. 4 TEM image of **a** SC **b** SCG

and gram-negative *Staphylococcus aureus* are displayed in Table 3.

The results and Fig. 5a, b, c and d confirm that the antibacterial activity of SCG was much higher than SC. The reason could be Ag nanoparticles capped with Chitosan/Glycine or Chitosan can interfere with mass transport across the cell wall, leading to bacterial mortality. Compared to SC, the SCG showed enhanced antibacterial activity due to the amino acid linking of glycine with chitosan. Stabilizing chitosan Ag nanoparticles were discovered to be somewhat active against microbes, and Akmaz et al. (Akmaz et al. 2013) also reported similar results. The amine functional groups in the Ag nanoparticles are probably the root cause. Further modification of chitosan with glycine enhances its efficacy due to the modified functional groups of chitosan.

The anti-fungal activity of SC and SCG was similarly conducted against *Aspergillus fumigates* MTCC 343 and *Candida albicans* MTCC227, whose results are shown in Table 4

Figure 6a, b, c and d shows the comparison between SCG and SC in which SCG showed better anti-fungal activity. The cross-linking of glycine and chitosan could be the cause of this. The remarkable anti-fungal action of SCG-NPs is assumed to be caused by the combination of the positive charge of the amino group in glycine with the negative charge of the fungus's components. SCG-NPs can prevent fungus growth by chelating various transitional metal ions, inhibiting enzymes, and preventing exchange with the medium (Shrifian-Esfahni et al. 2015).

Free radicals are produced in biological systems due to the interaction of biomolecules with molecular oxygen (Phaniendra et al. 2015). Anti-oxidant substances are therefore employed to counteract the ROS effect. The results are shown in Table 5

Table 3 Antibacterial activity of SC and SCG

Species	NPs	10 µ ml	20 µ ml	30 µ ml	40 µ ml
Staphylococcus aureus MTCC430	SC	11	15	15	17
	SCG	15	23	28	31
Escherichia coli MTCC739	SC	12	14	17	21
	SCG	15	23	28	31

SC and SCG showed scavenging rates ranging from 15 to 133%. The DPPH scavenging activity was higher than standard values (Table 5). The IC50 value for DPPH scavenging activity of synthesized SC was 92 µg ml $^{-1}$; while, the IC50 value for SCG was 133 µg ml $^{-1}$, respectively. The result showed that when compared to SC-NPs, SCGNPs displayed increased anti-oxidant activity. The binding of transition metal ion catalysts, peroxide decomposition, chain reaction inhibition, and continuing hydrogen abstraction are thought to be the mechanisms of action of SCG's anti-oxidant activity (Tamil Elakkiya et al. 2022). The presence of diverse phytochemical bio-reductive groups on the surface of the Ag NPs is responsible for the maximum anti-oxidant activity.

Mechanism of antibacterial and anti-oxidant activity of SCG

Antibacterial: The modification of chitosan with glycine enhances the interaction between the nanoparticles and bacterial cell membranes. Glycine, being a small amino acid, can improve the surface properties of chitosan, allowing for better adhesion to bacterial cells. This increased interaction facilitates the penetration of silver ions into the cells, leading to more effective antibacterial action (Cinteza et al. 2018; Dara et al. 2020). The combination of glycine-modified

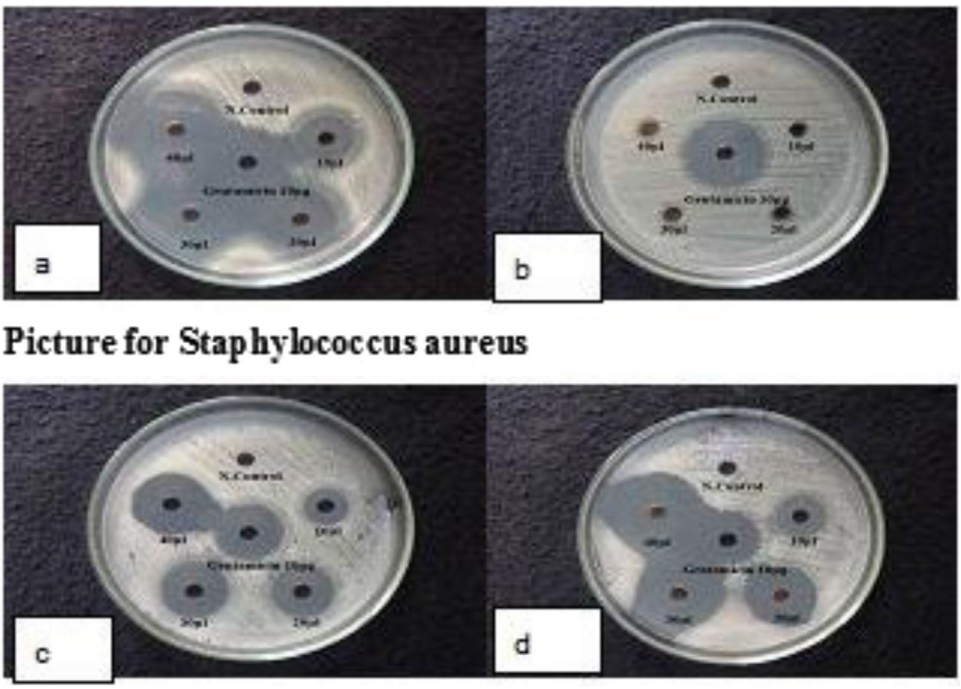


Fig. 5 **a** and **b**. Antibacterial activity of SCG, SC-*Staphylococcus aureus* **c** and **d**. Antibacterial activity of SC, SCG-*Escherichia coli*

Table 4 Anti-fungal activity of SC and SCG

Anti-fungal activity				
Candida albicans MTCC227				
µ ml	10	20	30	40
SC	0	10	12	13
SCG	10	12	13	14
Aspergillus fumigates MTCC343				
µ ml	10	20	30	40
SC	12	14	16	21
SCG	13	20	23	27

chitosan and silver nanoparticles can lead to synergistic antibacterial effects. Studies have shown that modifications like glycine can enhance the overall efficacy of the nanoparticles by improving their stability and biocompatibility while maintaining strong antibacterial properties (Zhang et al. 2023).

Anti-oxidant: Chitosan itself possesses inherent antioxidant properties due to its functional groups (e.g., amino and hydroxyl groups). When modified with glycine, these properties are enhanced, allowing Gly–Ch–Ag NPs to effectively scavenge free radicals and reduce oxidative stress in biological systems. This activity is crucial for protecting cells from damage caused by reactive oxygen species (ROS) (Song et al. 2011).

Response surface methodology

Experimental investigations were performed based on the CCD outputs for the optimization of the independent variables, and the responses of the runs are summarized in Table 6. It can be noticed that the maximum removal efficiency was obtained at pH 6 with higher contact time and lower initial concentrations.

The experimental results for 20 runs at various independent variables are summarized in Table 6 and the predicted values obtained from the CCD. It is worth noting that most of the experimental values coincided with the predicted values, and these observations propound that the developed model is reliable. The percentage removal of Pb^{2+} ion by SCG was found to be 93.5% at pH 6 with a contact time of 60 min and initial concentration of 15 mgL^{-1}. At optimal conditions (pH 6, time 60 min and initial concentration 100 mgL^{-1}) the removal efficiency was found to be 82% and the predicted values are also coinciding with the experimental values. Table 7 summarizes the findings of the analysis of variance used to establish the significance of the quadratic model, taking into account the dependability based on the experimental and predicted values.

The significance of the quadratic model can be understood based on the *p*-value and F-value obtained from the ANOVA. From Table 7, the *p*-value of the developed model is < 0.0001, suggesting that the model is significant. In addition, the *p*-value of independent variables and interaction among them for many were < 0.05, suggesting the significance of the key variables that influence the removal of Pb^{2+}

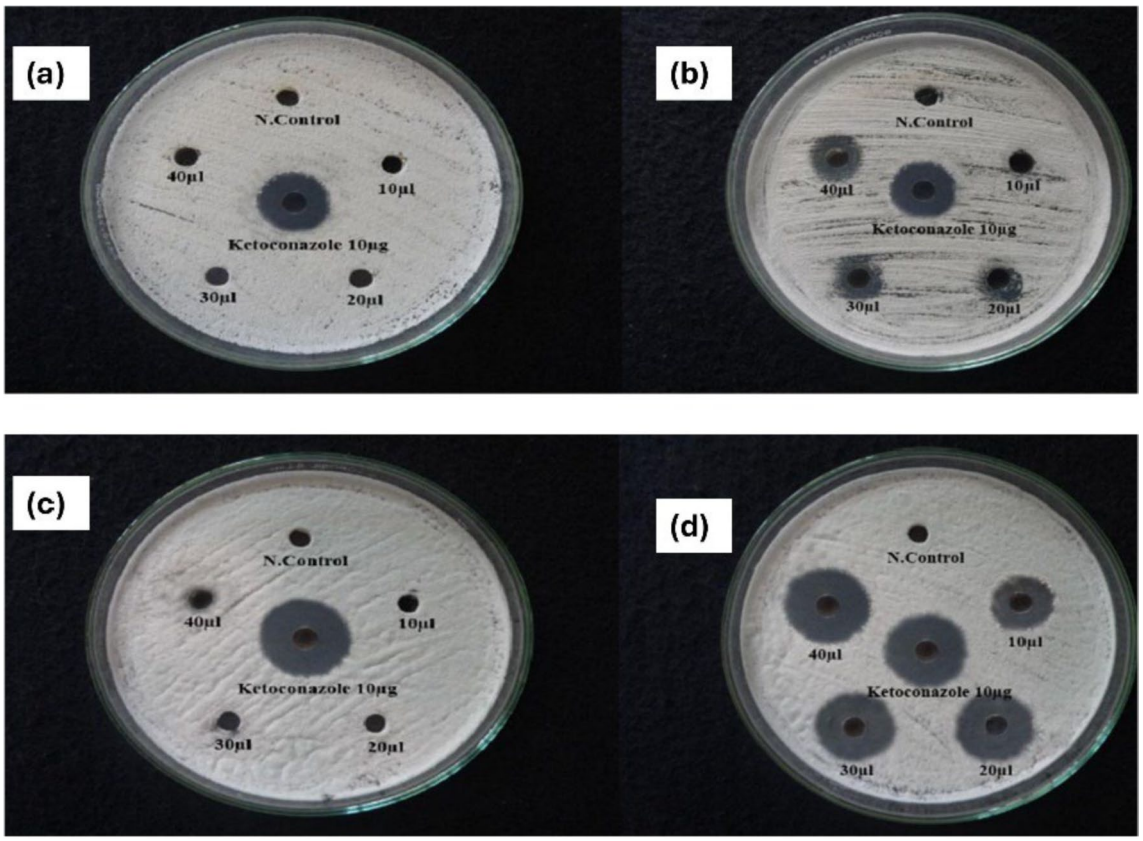


Fig. 6 **a** and **b**. Anti-fungal activity for SC, SCG-*Andida albicans* **c** and **d**. Anti-fungal activity for SC, SCG-*Aspergillus fumigates*

Table 5 Anti-oxidant activity of SC and SCG

DPPH	50	100	150	200	250	IC 50
SC	11	16	21	39	54	92
SCG	13	16	22	26	31	133

ions by SCG. The F-value was obtained to be 42.16 which high and higher F-values suggest the significance and better data fit to the developed model. The lack of fit that defines the inappropriateness of the model is found to be non-significant. The standard deviation was noted to be 5.25, and the correlation of variance was determined to be 8.68 and these low values suggest the reliability of the model and can be effective in the removal of Pb^{2+} ions by SCG (Gari and Kim 2015). Further, the correlation coefficient for this model was found to be 0.974, suggesting the model's applicability and the adjusted and predicted values were determined as 0.951 and 0.803, supporting the model's appropriateness. The adequate precision that defines how well the model responds and provides signals was found to be 20.4, which defines the adequate signal-to-noise ratio.

3D Surface plots

The 3D surface plots obtained as an output of the quadratic model graphically represent how the independent variables interact with each other and influence the removal efficiencies. Figure 7 represents the 3D surface plots obtained in this investigation. Figure 7a represents the 3D plot for the interaction of pH vs contact time, and it is noted that optimal pH is observed at pH 6 with an optimal contact time of 60 min. It is also observed that with higher contact time, the removal efficiency increases and is found to be saturated beyond 60 min. Figure 7b depicts the surface plot of pH vs initial concentrations. The interactions suggest that the removal efficiency is greater at lower initial concentrations at pH 6, and the removal declines with an increase in initial concentration. The interaction between contact time and initial concentration is shown in Fig. 7c, and it is noted that

Table 6 Experimental runs at variance independent variables

Run no	pH	Contact time	Initial concentration	Removal %	
				Experimental	Predicted
1	6	60	100	81.5	82.6
2	6	60	15	93.5	85.1
3	6	60	100	82.6	82.6
4	4	30	50	36.4	40.7
5	6	60	180	55.3	55.7
6	4	30	150	32.6	33.2
7	6	60	100	82.3	82.6
8	6	60	100	81.6	82.6
9	3	60	100	12.5	9.3
10	8	30	150	34.6	36.7
11	8	90	150	42.6	44.1
12	4	90	50	46.8	50.6
13	8	30	50	57.1	62.9
14	9	60	100	36.8	29.6
15	6	110	100	87.4	83.8
16	6	60	100	82.1	82.6
17	8	90	50	68.8	74.1
18	6	60	100	81.9	82.6
19	4	90	150	39.2	39.3
20	6	10	100	74.3	69.4

the independent variables interact interestingly with optimal conditions: higher contact times and lower initial concentrations. With higher contact time, the Pb^{2+} ions have sufficient time to interact with the SCG, thus maximizing removal efficiency. As the concentration increases, the active sites for binding diminish, resulting in lower efficiency.

Further, the predicted vs actual values were plotted as a graph, and it can be observed in Fig. 7d that the points are aligned in a straight line without much deviation. These alignments of points in the straight line propound the appropriateness and reliability of the model for removing Pb^{2+} ions by SCG. The 3D plot depicts only two independent variables' interaction and their results, but a cube could well represent how well the points of independent variables are distributed. Figure 8a shows the cube of three independent variables, points distribution and points are scattered. A maximum of 6 points are concentrated at the cube's center, suggesting the variables' optimal conditions. Further, the histogram shows the frequency of removal percentage being greater than 73% and a total of 9 runs out of 20 runs show higher removal efficiency (Fig. 8b).

Adsorption isotherms

The mathematical models provide valuable information in adsorption investigations regarding the adsorption process. Isotherms provide unique information on how the adsorbate and adsorbent bind. In view of the above, two isotherm models that are predominantly utilized for the adsorption of Pb^{2+} ions by metal nanoparticles were adopted for the equilibrium data. Figure S4 displays the isotherm plots, and Table 8 summarizes the corresponding constants and correlation coefficients. The higher K_f value 2.044 suggest that the SCG has high adsorption capacity and higher adsorption intensity (n) value of 129.8 is beyond the limits of the explanation of the model. The correlation coefficients of Freundlich isotherm (0.873) is moderate suggesting the moderate explanation of the adsorption process. However, it is observed that the correlation coefficient of

Table 7 Analysis of variance for the model developed for the removal of Pb^{2+} ions by SCG

Source	Sum of squares	*df*	Mean square	F-value	*p*-value
Model	10466.61	9	1162.96	42.16	< 0.0001
A-pH	571.90	1	571.90	20.73	0.0011
B-contact time	252.75	1	252.75	9.16	0.0127
C-initial concentration	1178.99	1	1178.99	42.75	< 0.0001
AB	0.9112	1	0.9112	0.0330	0.8594
AC	173.91	1	173.91	6.31	0.0309
BC	7.03	1	7.03	0.2549	0.6246
A^2	8102.51	1	8102.51	293.76	< 0.0001
B^2	65.20	1	65.20	2.36	0.1552
C^2	297.94	1	297.94	10.80	0.0082
Residual	275.82	10	27.58		
Lack of fit	274.94	5	54.99	12.43	0.987
Pure error	0.8800	5	0.1760		
Cor total	10742.43	19			
Std deviation	Adequate precision	R^2	Adjusted R^2	Predicted R^2	C.V%
5.25	20.4	0.974	0.951	0.803	8.68

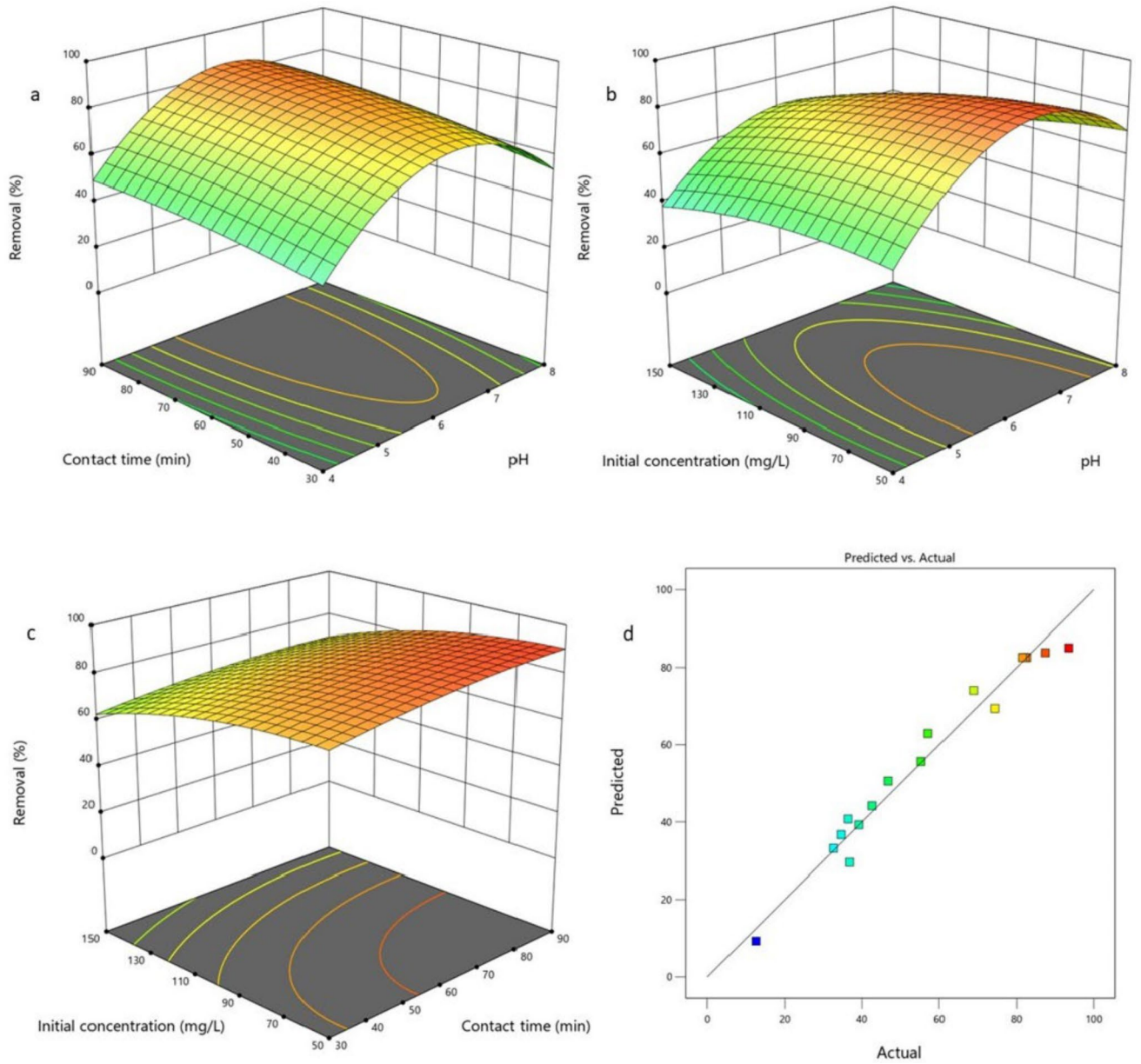


Fig. 7 3D surface plots **a** pH versus contact time, **b** pH versus initial concentration, **c** contact time versus initial concentration and **d** actual versus predicted plot

the Langmuir isotherm model (0.999) is close to one, propounding the model's applicability. The better fit of the Langmuir model is further bolstered by the loading capacity values, which were in close agreement with the experimental and theoretical values. The applicability of the model on the removal of the Pb^{2+} ions by SCG suggests that the Pb^{2+} ions form a uniform monolayer on the surface of the SCG. Similar results were reported for removing Pb^{2+} ions by silver nanoparticles (Jayachandra et al. 2016). Further to understand the adsorption mechanism by mean potential energy (E_s) D-R isotherm was applied to the equilibrium data. The E_s value was calculated to be 9.4 kJ/mol which suggest that the adsorption of Pb^{2+} ions by SCG is ion exchange.

Kinetics of adsorption

The rate of reaction provides the underlying process of adsorption of metal ions onto the adsorbent, and the kinetic data obtained by varying the time can be analyzed

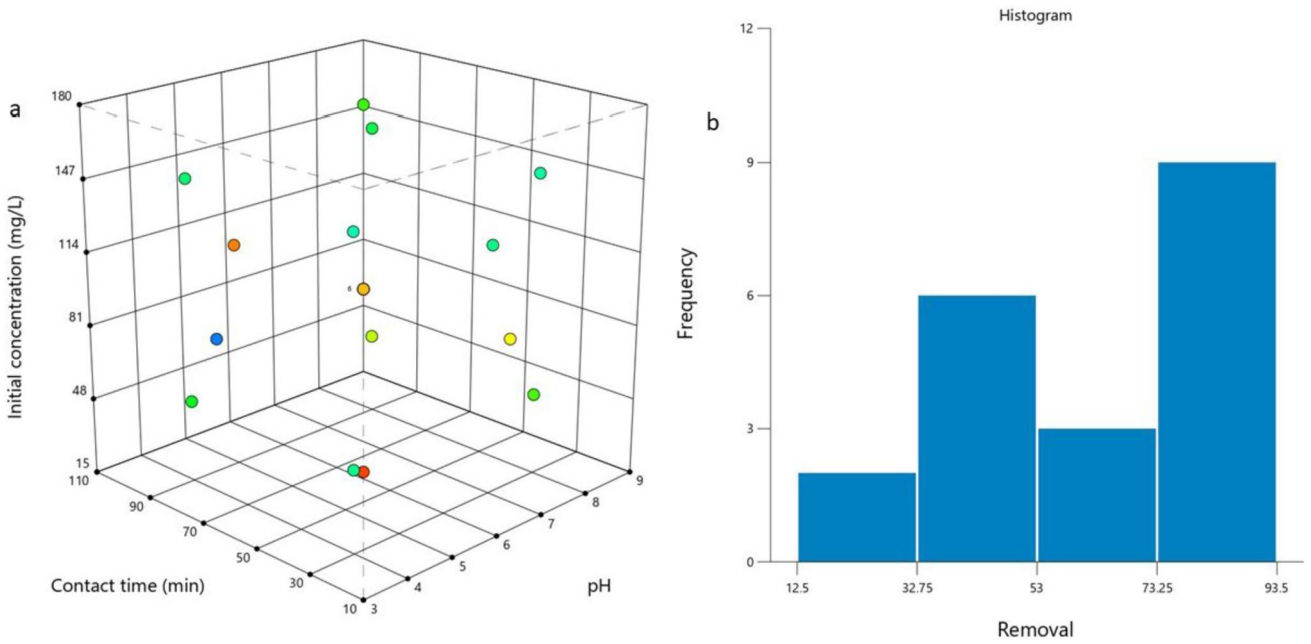


Fig. 8 **a** Cube distribution of points and **b** histogram of independent variables

Table 8 Langmuir and Freundlich isotherm constants for the removal of Pb^{2+} ions by SCG

Model	Equation	Parameters	Values
Freundlich	$\log q_{e=} \log K_f + \frac{1}{n} \log C_e$	K_f	2.044
		$1/n$	0.0077
		R^2	0.873
Langmuir	$\frac{C_e}{q_e} = \frac{1}{bV_m} + \frac{C_e}{V_m}$	b	0.949
		V_m	270.2
		R^2	0.999
D-R	$\ln q_e = \ln q_m - \beta\varepsilon^2$	K_D	5×10^{-9}
	$\varepsilon = RT \ln\left(1 + \frac{1}{C_e}\right)$	E_s	9.4
	$E_s = \frac{1}{\sqrt{2K_D}}$	R^2	0.806

Table 9 Kinetic parameters for the removal of Pb^{2+} ions by SCG

Model	Equation	Parameters	Values
Pseudo first order	$\ln\left(q_e - q_t\right) = \ln q_e - k_1 t$	k_1	0.533
		q_t	36.9
		R^2	0.996
Pseudo-second-order	$\frac{t}{q_t} = \frac{1}{k_2 q_e^2} + \frac{1}{q_e}$	k_2	0.037
		q_t	151.4
		R^2	0.999

with the kinetic models such as Pseudo first order (PFO), Pseudo-second-order (PSO) and intraparticle diffusion models. Model graphs from the kinetic data analysis are shown in Figure S5 and Table 9 summarize the corresponding correlation coefficients. The higher k_1 values suggest that the SCG has ability to quickly adsorb Pb^{2+} ions from aqueous solutions. The correlation coefficients of both models were very close to one, suggesting the better fit of both models and ability to explain the process. However, based on the theoretical loading capacities comparison with experimental values, PSO values were found to have good agreement and suggest that the transfer of electrons and chemisorption control the rate-limiting step should be the process of adsorption. However, if chemisorption should be the rate-limiting step, it has to satisfy several conditions, as reported by several studies (Lakshmipathy and Sarada 2016). A detailed investigation on these lines must be performed to validate the conditions. Intraparticle diffusion investigations were performed for the kinetic data, and the plot is shown in Fig. S6. It is noticed that the plot has a two-step, and the first step is steep suggesting the intraparticle diffusion and quick utilization of the active sites. This suggest that the surface active sites play a significant role in the adsorption process. The second step is the slow diffusion of the Pb^{2+} ions onto the surface of the SCG, and found to be saturated and flat. This indicates that the equilibrium is reached.

Thermodynamics of adsorption

The nature and spontaneity of the adsorbate getting adsorbed onto the adsorbents are essential to understanding the industrial applicability of the adsorbent.

The heat of adsorption is critical for understanding the adsorption efficiency, loading capacity, and nature of adsorption for an adsorbent. The equilibrium constant of adsorption (K_D) was calculated using Langmuir equilibrium parameter (b) using the below equation

$$K_D = b\left(\frac{L}{\text{mol}}\right).C_{\text{ref}}\left(\frac{\text{mol}}{L}\right).\frac{1}{\gamma'} \tag{5}$$

where K_D is the equilibrium constant C_{ref} is the molar concentration of the reference state and γ' is the activity coefficient calculated based on the ionic strength.

To investigate the factors for the removal of Pb^{2+} ions by SCG, the change in free energy ($\Delta G°$), enthalpy ($\Delta H°$), and entropy ($\Delta S°$) of the system were calculated using the following equations

$$\Delta G° = -RT \ln K_D \tag{6}$$

$$\Delta G° = \Delta H° - T\Delta S° \tag{7}$$

$$\ln K_D = \frac{\Delta S°}{R} - \frac{\Delta H°}{RT} \tag{8}$$

where R is gas constant and T is temperature.

The study revealed interesting findings regarding the change in free energy ($\Delta G°$) during the adsorption process (Table 10). Notably, $\Delta G°$ remained negative across all tested temperatures. However, the magnitude of these negative values decreased as the temperature rose. Negative $\Delta G°$ values indicate a spontaneous process, but the decreasing negativity suggests a decline in spontaneity with increasing temperature. This decline might be attributed to two factors: a weakening of the adsorption sites on the SCG surface and a corresponding increase in the kinetic energy of the Pb^{2+} ions within the solution. The negative enthalpy (ΔH) also signifies an exothermic process, where heat is released during adsorption. Furthermore, the positive entropy (ΔS) values point toward increased randomness associated with this heat release.

Regeneration and reusability investigations

It is essential to regenerate and reuse the adsorbents in order to establish their practical utility in the real time applications. In this study, efforts were made to regenerate and reuse the SCG for adsorption of Pb^{2+} ions from aqueous solution. The results of the investigations are shown in Fig. 9a. A total of four desorbing agents were tested for the regeneration of SCG and of four desorbing agents, HCl exhibited highest efficiency compared to CH_3COOH, NaOH and Na_2CO_3 agents. The higher efficiency exhibited by HCl is due to strength of the acid in producing hydronium ions compared to organic acid and bases. Hence, HCl was used as desorbing agents for further regeneration studies. The regenerated SCG was reused for five cycles and the removal efficiencies of each cycle are depicted in Fig. 9b. The removal efficiencies were found to be same for first two cycles and later found to decline. The decline in removal efficiency is due to repeated acid treatments which results in the weakening of the adsorption sites. These results suggest that SCG can be prolifically reused for two cycles without effecting its maximum removal efficiency.

Table 10 Thermodynamic parameters derived for the removal of Pb^{2+} ions by SCG

Temperature (K)	Change in free energy ($\Delta G°$)	Enthalpy ($\Delta H°$)	Entropy ($\Delta S°$)
303	− 14,351	− 5570	1424
313	− 12,312		
323	− 11,503		

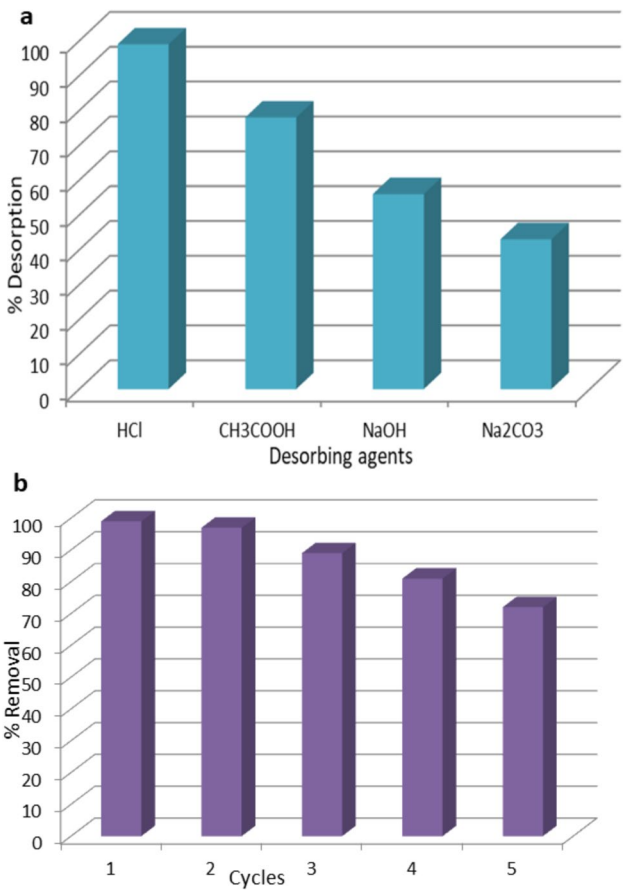


Fig. 9 Regeneration and reuse of SCG nanoparticles

Comparison of Pb^{2+} ion adsorption by SCG with other divalent metal ions and adsorbents

Investigations were performed to understand the selectivity and preferential uptake of Pb^{2+} ions in comparison with other divalent metal ions such as Zn^{2+}, Cu^{2+}, Ni^{2+}, and Cd^{2+} ions from aqueous solutions. The loading capacities of the selected divalent metal ions are represented in Table 11. It is noticed that the Pb^{2+} ions have preferential uptake compared to other tested metal ions and this is due to the larger ionic radius and high charge density favoring the preferential surface interactions of Pb^{2+} ions. In addition to the above, heavier atomic nature of Pb^{2+} ions results in higher polarizability resulting in the better interactions with the electron cloud of the SCG. Further, the loading capacity of the SCG was compared with other Ag NPs synthesized using various sources and tabulated in Table 12. It is noticed that the SCG has high adsorption capacity compared to several other Ag NPs and this is due to the surface modification and functionalization that enhanced the Pb^{2+} ions adsorption. In addition to that the antimicrobial activity is also compared and presented.

Mechanism of adsorption

The mechanism of adsorption is essential to understand how the Pb^{2+} ions are adsorbed on to the surface of the SCG. In this study, efforts were made to deduce the mechanism of adsorption. The point zero charge of the SCG was determined to be pH 5.5 and above this pH, the SCG would exhibit negative surface. The negative surface will attract positively charged Pb^{2+} ions for adsorption due to electrostatic attraction. Further the desorption and regeneration investigation suggest that ion exchange is possible with H^+ ions getting exchanged with Pb^{2+} ions. The mean potential energy (E_s) value was determined to be 9.4 kJ/mol suggesting the ion exchange mechanism of adsorption. The glycine functionalization onto the surface of chitosan modified silver nanoparticles provide $–NH_2$ and –COOH where H^+ ions can be exchanged with Pb^{2+} ions. The electrostatic and ion exchange synergistically enhance the adsorption of Pb^{2+} ions by SCG. The electrostatic force attract the Pb^{2+} ions closer to the surface and facilitate the ion exchange process.

Table 11 Loading capacities of SCG toward various divalent metal ions

Metal ion	Adsorption capacity (mg g^{-1})
Zn^{2+}	132.5
Ni^{2+}	160.2
Cu^{2+}	166.4
Cd^{2+}	201.8
Pb^{2+}	270.2

Conclusion

In this study, SC NPs and SCG NPs were synthesized successfully. The synthesized SCG exhibits significant anti-oxidant activity and appears promising and effective antibacterial and anti-fungal agent. These properties may prove valuable in creating novel drugs for biomedical purposes. The batch adsorption studies on removing Pb^{2+} ions by SCG NPs were executed by developing CCD based on RSM. The developed model was found to be significant with a p-value < 0.0001. The F-value, correlation coefficients and adequate precision support the model's applicability for effectively removing Pb^{2+} ions by SCG with a loading capacity of 270.2 mg g^{-1}. The isotherm and kinetic investigations suggest that the system follows Langmuir and Pseudo second-order kinetic models with high correlation coefficients. Thermodynamic investigations confirmed the spontaneity and exothermic nature of the present process. Overall, the silver chitosan–glycine-modified nanoparticles

Table 12 Adsorption capacity and antimicrobial activity comparison of SCG with other Ag NPs

S. no	Nanomaterial	Loading capacity Pb^{2+} ions (mg g^{-1})	Antimicrobial activity (ZOI)		References
			S. Aureus	*E. Coli*	
1	Ag NPs	105.4	–	–	Huacai et al. (2016)
2	Nano-silversol-coated activated carbon	23.8	–	–	Kumar et al. (2010)
3	Silver nanoparticles grafter CNT's	18.7	–	–	Neelgund et al. (2022)
4	Peel extract mediated Ag NPs	42.7	–	–	Aboelghait et al. (2024)
5	Biogenic Ag NPs	–	20.0	15.0	Sana et al. (2024)
6	Leaf extract mediated Ag NPs	–	12.5	11.6	Partha et al. (2023)
7	Root extract mediated Ag NPs	–	12.2	12.2	Venkatachalam et al. (2024)
8	Leaves extract mediated Ag NPs	–	10.8	12.3	Vinay et al. (2024)
9	Chitosan glycine-modified Ag NPs	270.2	31.0	31.0	This study

are an effective anti-oxidant and adsorbent that can have versatile applications.

Supplementary Information The online version contains supplementary material available at https://doi.org/10.1007/s11696-024-03842-3.

Author contributions SK contributed to data collection; AG contributed to result interpretation; RL contributed to methodology; DA contributed to result evaluation; SA contributed to draft manuscript preparation; MG contributed to analysis and interpretation of results; KKS contributed to study conception and design.

Funding Open Access funding provided by the Qatar National Library. The authors extend their appreciation to Researchers Supporting Project number (RSP2025R165), King Saud University, Riyadh, Saudi Arabia.

Data availability The paper contains all necessary information, and the corresponding author can provide any further information upon request.

Declarations

Conflict of interest The authors declare that they have no conflict of interest.

Ethical approval Not applicable.

Open Access This article is licensed under a Creative Commons Attribution 4.0 International License, which permits use, sharing, adaptation, distribution and reproduction in any medium or format, as long as you give appropriate credit to the original author(s) and the source, provide a link to the Creative Commons licence, and indicate if changes were made. The images or other third party material in this article are included in the article's Creative Commons licence, unless indicated otherwise in a credit line to the material. If material is not included in the article's Creative Commons licence and your intended use is not permitted by statutory regulation or exceeds the permitted use, you will need to obtain permission directly from the copyright holder. To view a copy of this licence, visit http://creativecommons.org/licenses/by/4.0/.

References

Aboelghait KM, Abdallah WE, Abdelfattah I, El-Shamy AM (2024) Green synthesis of silver nanoparticles by waste of Murcott Mandarin peel as a sustainable approach for efficient heavy metal removal from metal industrial wastewater. Sep Purif Technol 347:127609

Akmaz S, Adjgüze L, Yasar ED, Erguven MO (2013) The effect of Ag content of the chitosan-silver nanoparticle composite material on the structure and antibacterial activity. Adv Mater Sci Eng 2013:1–6

Azmi SNH, Al-Jassasi BMH, Al-Sawafi HMS (2021) Optimization for synthesis of silver nanoparticles through response surface methodology using leaf extract of *Boswellia sacra* and its application in antimicrobial activity. Environ Monit Assess 193:497

Azza A, Abu-Hussen (n.d.) Synthesis and spectroscopic studies on ternary bis-Schiff-base complexes having oxygen and/or nitrogen donors. J Coord Chem, 59(2): 157–176

Balalakshmi C, Alharbi NS, Kadaikunnan S, Khaled JM, Alanzi KF, Gopinath K, Arumugam A, Govindarajan M (2020) Development of chitosan/agar-silver nanoparticles-coated paper for antibacterial application. Green Process Synth 9(1):751–759

Cinteza LO, Scomoroscenco C, Voicu SN, Nistor CL, Nitu SG, Trica B, Jecu ML, Petcu C (2018) Chitosan-stabilized Ag nanoparticles with superior biocompatibility and their synergistic antibacterial effect in mixtures with essential oils. Nanomaterials (Basel) 8(10):826

Constantin M, Lupei M, Bucatariu SM, Pelin IM, Doroftei F, Ichim DL, Daraba OM, Fundueanu G (2023) PVA/chitosan thin films containing silver nanoparticles and ibuprofen for the treatment of periodontal disease. Polymers. 15: 4

Dandu Kamakshi Gari VR, Kim M (2015) Removal of Pb(II) using silver nanoparticles deposited graphene oxide: equilibrium and kinetic studies. Monatsh Chem 146:1445–1453

Dara PK, Mahadevan R, Digita PA (2020) Synthesis and biochemical characterization of silver nanoparticles grafted chitosan (Chi-Ag-NPs): in vitro studies on antioxidant and antibacterial applications. SN Appl Sci 2:665

El-Naggar ME, Farag AS, Abeer AAS, Rehab MH, Gamila HA (2018) Cationic starch: safe and economic harvesting flocculant for microalgal biomass and inhibiting *E. coli* growth. Int J Biol Macromol 116:1296–1303

Gupta KC, Ravikumar MNV, Fawzi HJ (2015) Chitosan-glycine cross-linked microspheres for controlled release of isoniazid. J Mod Chem Chem Technol 6(3):7–12

Hassan F, Nasrin M, Hamid M, Fariba M (2024) Methanolic extract of *Arctium lappa* and *Eryngium billardieri*: anti diabetic, antibacterial, anticancer and silver nanoparticles biosynthesis evaluation. Biocatal Agric Biotechnol 57:103079

Hosseini SJ, Aghaie H, Ghaedi M, Dashtian K, Purkait MK (2016) Lead (II) adsorption from aqueous solutions onto modified ag nanoparticles: modeling and optimization. Environ Prog Sustain Energy 35:743–749

Huacai G, Tingting H, Xiaodong C (2016) Selective adsorption of lead on grafted and crosslinked chitosan nanoparticles prepared by using Pb^{2+} as template. J Hazard Mater 308:225–232

Illum L (1998) Chitosan and its use as a pharmaceutical excipient. Pharm Res 15:1326–1331

Jayachandra R, Lakshmipathy R, Rajasekhara Reddy S (2016) Hydrophobic D-galactose based ionic liquid for the sequestration of Pb2+ ions from aqueous solution. J Mol Liq 219:1172–1178

Kamlesh K, Usha R (2011) Controlled Release of Metformin hydrochloride through crosslinked blends of chitosan-starch. Adv Appl Sci Res 2(2):48–54

Kumar M, Muzzarelli RAA (2004) Chitosan chemistry and pharmaceutical perspectives. Chem Rev 104:6017–6084

Kumar PS, Vincent C, Kirthika K, Kumar KS (2010) Kinetics and equilibrium studies of Pb^{2+} in removal from aqueous solutions by use of nano-silversol-coated activated carbon. Braz J Chem Eng 27(2):339–346

Lakshmipathy R, Sarada NC (2016) Metal ion free watermelon (*Citrullus lanatus*) rind as adsorbent for the removal of lead and copper ions from aqueous solution. Desalin Water Treat 57:15362–15372

Lena R (2023) Microalgae with active biological metal-nanoparticles as a novel food Biosynthesis, characterization and bioavailability investigation—Review. Trends Food Sci Technol 139:104127

Madihally SV, Matthew HWT (1999) Porous chitosan scaffolds for tissue engineering. Biomaterials 20(12):1133–1142

Mahdi G, Orkideh S, Mohsen A (2020) Adsorptive removal of lead (II) ion from water and wastewater media using carbon-based nanomaterials as unique sorbents: a review. J Environ Manage 254:109814

Mengistu M, Molla T, Atnafu G, Basavaia K (2024) Biosynthesis, characterization and study of the application of silver nanoparticle for

4-nitrophenol reduction, and antimicrobial activities. Biotechnol Rep 42:e00838
Mohammed FH, Mohsen MA, Abdel-Rahman A, Samar R (2017a) Functionalization of magnetic chitosan particles for the sorption of U(VI), Cu(II) and Zn(II)—hydrazide derivative of glycine-grafted chitosan. Materials 10:539
Mohammed FH, Mohsen MA, Adel AH, Abdel R, Samar R, Heba R, Shengye W (2017b) Thierry vincent and eric guibal, supplementary materials: functionalization of magnetic chitosan particles for the sorption of U(VI), Cu(II) and Zn(II)—hydrazide derivative of glycine grafted chitosan. Materials 10:539
Mrinalini P, Mallika S (2024) Biosynthesis of gold nanoparticles using aqueous extract of *Ricinus cummunis* leaves to augment catalytic degradation of organic dyes and study of its antifungal and antibacterial activities. Particuology 87:87–98
Nafisur R, Nabila K (2023) Synthesis and characterization of 1-phenylisatin incorporated chitosan/PEG nanoparticles: Interaction with bovine serum albumin and application in drug delivery. J Drug Deliv Sci Technol 86:104738
Nafisur R, Poornima V, Mohd N (2021) Synthesis and characterization of polydopamine/hydrous zirconium oxide composite and its efficiency for the removal of uranium (VI) from water. Environ Nanotechnol Monit Manag 15:100458
Nafisur R, Monika B, Mohd N, Syed N, Hejaz A (2024) Performance assessment of graphene oxide decorated with silver nanoparticles as adsorbent for removal of metformin from water: equilibrium modeling, kinetic and thermodynamic studies. Next Mater 3:100046
Neelgund GM, Aguilar SF, Kurkuri MD, Rodrigues DF, Ray RL (2022) Elevated adsorption of lead and arsenic over silver nanoparticles deposited on poly(amidoamine) grafted carbon nanotubes. Nanomaterials 12(21):3852
Ohiduzzaman Md, Khan MNI, Khan KA, Bithi P (2024) Biosynthesis of silver nanoparticles by banana pulp extract: characterizations, antibacterial activity, and bioelectricity generation. Heliyon 10(3):e25520
Panos I, Acosta N (2008) New drug delivery systems based on chitosan. Curr Drug Discov Techno 5:333–341
Partha PS, Kailash B, Pranjal KB (2023) Green synthesis of silver nanoparticles using *Murraya koenigii* leaf extract with efficient catalytic, antimicrobial, and sensing properties towards heavy metal ions. Inorg Chem Commun 152:110676
Phaniendra A, Jestadi DB, Periyasamy L (2015) Free radicals: properties, sources, targets, and their implication in various diseases. Indian J Clin Biochem 30:11–26
Pradip KD, Joydeep D, Tripathi VS (2004) Chitin and chitosan:chemistry, properties and applications. J Sci Ind Res 63:20–31
Prasitsilp M, Jenwithisuk R, Kongsuwan K, Damrongchai N, Watts P (2000) Cellular responses to chitosan in vitro: the importance of deacetylation. J Mater Sci Mater Med 11(12):773–778
Praveenkumar K, Rabinal MK, Kalasad MN, Sankarappa T, Bedre MD (2014) Chitosan capped silver nanoparticles used as pressure sensors. J Appl Phys 5:43–51
Sana I, Hajera G, Nargis J, Naeem K, Riaz U, Ahmed B, Tan WN, Joon HH, Rehana M (2024) Biogenic salvia species synthesized silver nanoparticles with catalytic, sensing, antimicrobial, and antioxidant properties. Heliyon 10(4):e25814
Seid RF, Fuat T, Dagmara B, Zahra M, Maryam S, Hajar H, Shruti R, Anbazhagan S, Myeong-Hyeon W, Rubiya K, Enayati MH, Hadis R (2023) Metal nanoparticles and carbohydrate polymers team up to improve biomedical outcomes. Biomed Pharmacother 168:115695
Shahid W, Haroon Muhammad A, Maham K, Tariq K, Chandran K, Soon-Il Y (2024) Green synthesis and antibacterial assessment of chitosan/silver nanocomposite conjugated with tobramycin against antibiotic resistant *Pseudomonas aeruginosa*. Arab J Chem 17(1):105458
Sharma VK, Yngard RA, Lin Y (2009) Silver nanoparticles: green synthesis and their antimicrobial activities. Adv Colloid Interf Sci 145:83–96
Shrifian-Esfahni A, Salehi MT, Nasr-Esfahni M, Ekramian E (2015) Chitosan-modified superparamgnetic iron oxide nanoparticles: design, fabrication, characterization and antibacterial activity. Chemik 69:19–32
Song Y, Du B, Zhou T, Han B, Yu F, Yang R, Hu X, Ni Y, Li Q (2011) Optimization of extraction process by response surface methodology and preliminary structural analysis of polysaccharides from defatted peanut (Arachis hypogaea) cakes. Carbohydr Res 346:305
Suba K, Easwaramoorthi D, Karthik K, Andal G, Lakshmipathy R, Khadijah MK, Nayef S, Almuaikel ILR (2022) Pisonia Alba assisted synthesis of nano silver for wound healing activity. Bioinorg Chem Appl 2022:1775198
Tamil Elakkiya G, Balaji GL, Harihara P, Lakshmipathy R (2022) Synthesis of silver nanoplates using regenerated watermelon rind and their application. Mater Today: Proc 55:240–245
Varshosaz J (2007) The promise of chitosan microspheres in drug delivery systems. Expert Poin Drug Deliv 4:263–273
Venkatachalam B, Chinnasamy R, Dhanarajan A, Abdulwahed FA, Ranjith R (2024) Green synthesis of silver nanoparticles using Pandanus tectorius aerial root extract: characterization, antibacterial, cytotoxic, and photocatalytic properties, and ecotoxicological assessment. Inorg Chem Commun 168:112882
Vinay VK, Naveen KK, Lokanadhan G, Usha KM, Venkateswara RK, Sudhakar P, Suresh BNK (2024) Green synthesis of silver nanoparticles from *Hibiscus tiliaceus* L. leaves and their applications in dye degradation, antioxidant, antimicrobial, and anticancer activities. S Afr J Bot 168:476–487
Wen Z, Jiaojiao L, Kaixiang J, Wenlong L, Xuefeng QL (2015) Chenrui fabrication of functional PLGA-based electrospun scaffolds and their applications in biomedical engineering. Mater Sci Eng C 59:1181–1194
Zhang Z, Zhao Y, Hu Z, Si Z, Yang Z (2023) 2-Pyridinecarboxaldehyde-modified chitosan-silver complexes: optimized preparation, characterization, and antibacterial activity. Molecules 28:6777

Publisher's Note Springer Nature remains neutral with regard to jurisdictional claims in published maps and institutional affiliations.